Magnetoresistive Sensors

H. Hauser, G. Stangl, W. Fallmann, R. Chabicovsky, K. Riedling

Institut für Industrielle Elektronik und Materialwissenschaften
TU Wien, Gusshausstrasse 27/366, A-1040 Vienna, Austria

Depending on the angle between magnetisation and current density in a thin permalloy film, the anisotropic magnetoresistive effect is utilised for high performance sensors. Both the parameters of the sputtering process and the sensor layout have to be optimised. Aiming a magnetic field resolution of some nT in a frequency range from 0 – 1 kHz, the results of Wheatstone bridge circuits are discussed.

Introduction

The magnetoresistive effect is the change of the resistivity of a material due to a magnetic field; it has been discovered by Thomson in 1856 [1]. The improvement of the technology of thin ferromagnetic films (with a thickness of 10 – 50 nm) and the utilisation of the Anisotropic Magnetoresistive (AMR) effect led to an increasing technical interest in this effect. Furthermore, a Giant Magnetoresistive (GMR) effect [2] has been discovered, which is based on the weak coupling between separate thin ferromagnetic films. The maximum resistivity change is up to 80% with the GMR effect, albeit at very high magnetic fields only.

AMR sensors feature a high sensitivity at weak magnetic fields and a small consumption of energy. Their maximum change of resistance is of the order of 3 – 4 %. These sensors can be produced in large quantities and very cost-efficiently if the processes required for their production can be handled reproducibly. Magnetoresistive sensors are used today, for example, in reading heads of magnetic data storage systems such as hard disks. They could find much wider spread applications, though, e.g., for measurements of the Earth's magnetic field, as a gradiometre, a compass, a position sensor, or for measurements of biomagnetic fields.

The sensors require thin ferromagnetic films (e.g., permalloy) with a magnetic anisotropy. There is a *hard axis* with a high requirement of magnetisation energy in one direction in the plane of the film, and, orthogonal to the hard axis in the plane of the film, an *easy axis* which indicates the magnetic preference direction. The sensitivity of the sensor depends on the width of the magnetic hysteresis, as indicated by the coercivity H_c. A second key parameter for AMR films is the relative change of the resistivity, $\Delta\rho/\rho$. This is the change of resistivity if the magnetisation vector is rotated by 90 degrees from the direction of the easy axis due to an external magnetic field.

Today, the technically most important sensors for magnetic fields are induction coils, Hall sensors, magnetoresistive and AMR sensors, fluxgates, and Superconducting Quantum Interference Devices (SQUIDs). The following Table 1 compares typical parameters of these sensors. Table 1 gives approximate values only; the maximum flux resolution depends, in general, also on the frequency. It decreases for all sensors, except

for AMR sensors, with decreasing frequency. This effect is most pronounced for the induction coils.

Sensor type:	min. B	max. B	Frequency range
Induction coils	100 fT	unlimited	0.1 mHz – 1 MHz
Hall sensors	10 nT	20 T	0 – 100 MHz
Magnetoresistive Sensors	100 pT	100 mT	0 – 100 MHz
Fluxgates	10 pT	1 mT	0 – 100 MHz
SQUIDs	5 fT	1000 nT	0 – 100 kHz

Table 1: A comparison of various magnetic sensors.

There are primary and secondary parameters of sensors: The *primary parameters* (e.g., range, band width, accuracy, resolution, linearity, hysteresis of the output signal) refer directly to the measured parameter. The *secondary parameters* (e.g., geometry, spatial resolution, working and storage temperature, chemical sensitivity, impedance, reliability, power consumption, and price) include the environment of the application and economic aspects.

Theory of the AMR sensor

The theory of the AMR sensor is based on the complex ferromagnetic processes in a very thin film. Some of the effects involved may be simplified for an easier mathematical treatment. First, the assumption is justified that the magnetisation M in a ferromagnetic material always has the magnitude of the saturation magnetisation M_S but only changes its direction. Second, the complex theory of the AMR effect (there is also an isotropic MR effect which is utilised in semiconducting layers) can be split into two simpler parts, namely, the relation between the electric resistivity and the direction of the magnetisation, and the relation between the direction of the magnetisation and an externally applied magnetic field.

Anisotropic magnetoresistive effect

The physical origin for the anisotropic magnetoresistive effect is the different shift of the energy levels of electrons with a positive and negative spin, respectively, under the influence of a magnetic field. This leads to a shift in the Fermi levels. It has not been possible yet to calculate these effects satisfactorily; the difference to experimental data is still about one order of magnitude [3]. Therefore, the most important parameters are determined experimentally.

It has been shown that the electric resistance R can be derived with a simple theory from the angle Θ between the electric current density and the magnetisation (see Fig. 1 (a)):

$$R(\Theta) = \rho_{0,n} \frac{l}{bd} + \Delta\rho \frac{l}{bd} \cos^2 \Theta = R_{0,n} + \Delta R \cos^2 \Theta \qquad (1)$$

In equation 1, $\rho_{0,n}$ and $\Delta\rho$ are material constants, l is the length of the resistive strip, b, its width, and d, its thickness. In general, l > b >> d. $R_{0,n}$ is the resistance perpendicular

to the magnetisation, and ΔR is the maximum change of resistance due to the magnetic field. For a current I in x direction, a voltage U_x results:

$$U_x = \rho_{0,n} I \frac{l}{bd} + \Delta\rho I \frac{l}{bd} \cos^2 \Theta \tag{2}$$

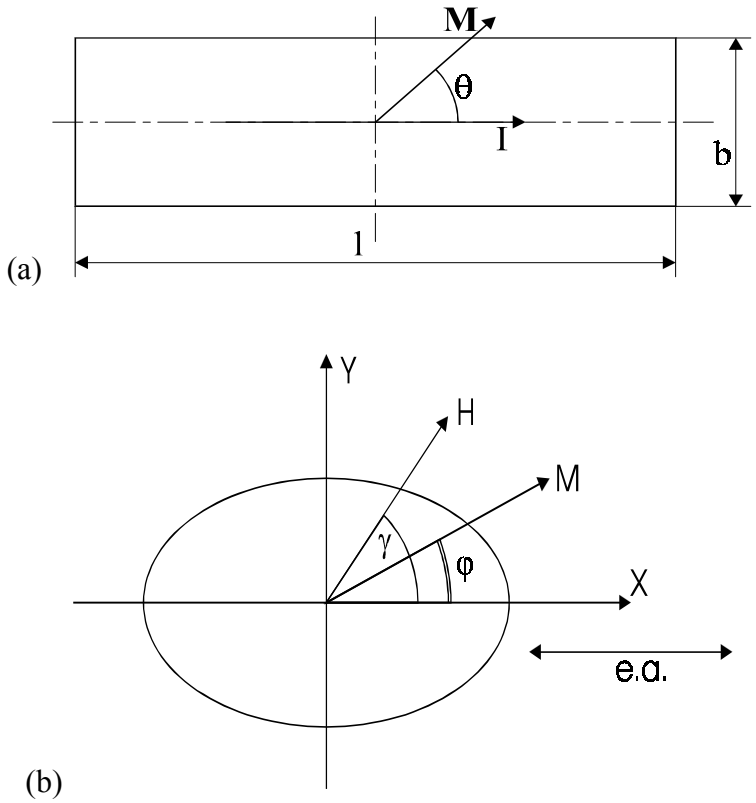

Fig. 1: (a) Geometry of a strip with magnetisation M and current direction I. (b) Geometry of an elliptically shaped thin film; the *easy axis* was assumed to be in parallel to the x axis.

It should be noted that there is also a voltage U_y perpendicular to the direction of current flow. Due to its similarity to the Hall effect, this effect is called *planar Hall effect*. It should not be mistaken for the common Hall effect, though, because its origin is totally different: In the common Hall effect, a voltage change is effected due to a magnetic field perpendicular to the film; for the planar Hall effect, the magnetic field is in the same plane as the current flow. The planar Hall effect is rarely used for practical purposes because the voltages involved are very small.

Magnetisation by an external field

The magnetisation M in the film is in a direction of minimum total energy. The most important energies involved are the energy of the external field, the anisotropy energy of the material (magnetocrystalline anisotropy energy), and the demagnetising energy (shape anisotropy energy). Most energy contributions depend on the direction. This implies that the energy required for rotating M into a given direction can be visualised by a three-dimensional energy area [4].

The spontaneous magnetisation M_S will lie in a direction with a minimum energy. The magnetocrystalline anisotropy energy area of iron has six easy axes (i.e., energy minima) in the direction of the edges of the crystal cube. Nickel has eight easy axes in the volume diagonals of the unit cell. In addition, the total energy depends on mechanical stress [5] and on the geometry. The energy planes of permalloy (Ni:Fe 81:19) are more complicated. There are 16 easy axes. However, the magnetostriction constant is close to zero in permalloy, i.e., the magnetisation has no effect on the crystal lattice dimensions.

With the total anisotropy field $H_0 = 2K/\mu_0 M_S$ (with the anisotropy constant K), the angle φ between M and the easy axis (x direction) results for $H_x = 0$ as:

$$\sin\varphi = \frac{H_y}{H_0} \tag{3}$$

for $-1 < H_y/H_0 < 1$. Outside of this range, $\sin\varphi = \mathrm{sign}\left(H_y / H_0\right)$.

Magnetoresistive sensors

The calculation of the angle Θ between M and the easy axis and the dependence of the electric resistance on the direction of M will be combined now to evaluate the sensor. We introduce the new resistances $R_{0,p}$ and R_0:

$$R_{0,p} = R_{0,n} - \Delta R \tag{4}$$

$$R_0 = R_{0,n} + \frac{\Delta R}{2} = \frac{R_{0,p} + R_{0,n}}{2} \tag{5}$$

R_0 is therefore the average resistance. We can calculate the characteristics of a simple AMR sensor using these new parameters. Figure 2 (a) depicts the dependence of the resistance on the angle between current flow and magnetisation. Equations (2) and (4) result in the resistance $R(\Theta)$:

$$R(\Theta) = R_{0,p} - \Delta R \sin^2\Theta \tag{6}$$

Equation (3) permits to calculate the resistance in dependence of the field H_y which is to be measured. Figure 2 (b) illustrates this dependence. For real measurements, the magnetisation M turns completely into the hard axis for very strong fields only. Therefore, there is a smooth transition into the saturation resistance:

$$R\left(H_y\right) = R_{0,p} - \Delta R\left(\frac{H_y}{H_0}\right)^2 \tag{7}$$

for $|H_y| \le H_0$ and

$$R\left(H_y\right) = R_{0,n} \tag{8}$$

for $|H_y| > H_0$. The resistance exhibits a strongly non-linear dependence on the external field. Furthermore, the sensitivity $\mathrm{d}R/\mathrm{d}H_y$ is very small in the proximity of the origin (and disappears entirely for $H_y = 0$). A further disadvantage of this setup is that the sign of H_y can not be determined since R is a function of H_y^2.

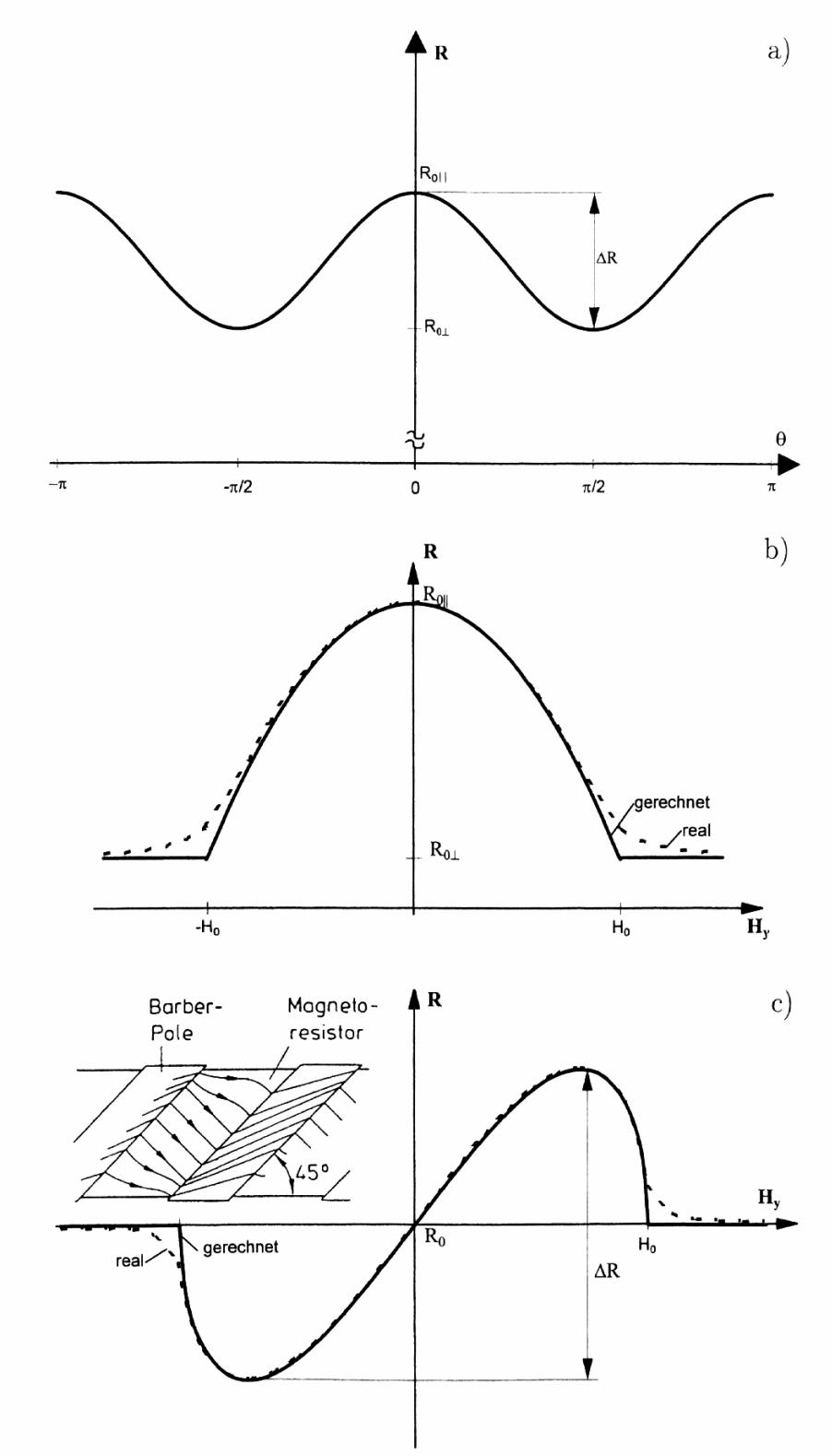

Fig. 2: (a) Resistance in x direction as a function of the angle Θ between the current I and the magnetisation M. (b) Resistance of a thin ferromagnetic film as a function of the transversal field H_y. (c) Current flow in a barber pole structure, and resistance R of a thin ferromagnetic film with a barber pole structure as a function of the transversal field H_y.

Barber pole

In order to alleviate these disadvantages, barber pole structures[1] have been introduced. Barber pole structures consist of a series of strips of high electrical conductivity that force the current flow into an angle of 45° with respect to the *x* axis, and therefore to the easy axis. Figure 2 (c) shows that the current paths are distorted at the edges of the barber poles. An optimum layout of width and distance of the barber poles is therefore crucial [7]. The well-conducting strips reduce the total resistance; they also reduce the active part of the surface where resistance changes contribute to the sensor signal.

Mathematically, barber poles are represented by introducing an additional angle ψ = 45°, which represents the angle between the easy axis and the current. The angle Θ is in this case:

$$\Theta = \varphi - \psi \tag{9}$$

The characteristics of a barber-pole AMR sensor result therefore as:

$$R(H_y) = R_0 + \Delta R \frac{H_y}{H_0} \sqrt{1 - \left(\frac{H_y}{H_0}\right)^2} \tag{10}$$

A graphic representation of the characteristics of an AMR sensor with barber poles is shown in Fig. 2 (c). For $H_y < H_0/2$, it is fairly linear with a non-linearity of less than 5%. This behaviour is only valid if the spontaneous magnetisation without an external field is in the positive *x* direction. The change of resistance changes its sign if the spontaneous magnetisation is flipped to the negative *x* direction. Flipping the spontaneous magnetisation can be utilised for determining the value of R_0 accurately as the arithmetic mean value of the two resistance values before and after flipping.

In order to convert the resistance changes into a voltage without a dc component, the sensor is realised as a Wheatstone bridge with four individual resistors. This approach demonstrates one more advantage of barber pole structures: By using barber poles under 45° and 135°, respectively, resistors with a positive and a negative ΔR in the linear range can be realised. In order to obtain a maximum output voltage, two diagonally opposite resistors have barber poles under 45°, and the other two, under 135° (see Fig. 3). This setup also compensates for a temperature dependence of the resistors.

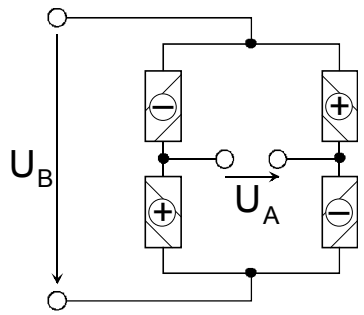

Fig. 3: Wheatstone bridge with four magnetoresistive devices. "+" indicates barber poles under 45°, and "–", under 135°.

[1] Named after the sign of a barber shop which looks very similar.

Sensitivity and measurement range

The output voltage of a Wheatstone bridge can be described by:

$$U_A = U_B \frac{\Delta R}{R_0} \frac{H_y}{H_0} \sqrt{1 - \left(\frac{H_y}{H_0}\right)^2} \tag{11}$$

The sensitivity[2] of the entire sensor results in:

$$S_0 = \frac{\Delta R}{R_0} \frac{1}{H_0} \tag{12}$$

The sensitivity can thus be increased by using materials with a high AMR effect and with a low characteristic field H_0. The sensors exhibit linear behaviour with an error of less than 5% within a range of $-H_0/2$ to $H_0/2$.

It is possible, though, to increase the measurement range arbitrarily by applying a compensating magnetic field (i.e., by a null-compensation of the bridge). Since the sensor always operates at zero field, its non-linearity has no effect. The maximum resolution depends in this case on the stability of the magnetic film.

Furthermore, the layout of the magnetoresistive elements forming a Wheatstone bridge has to be optimised. Achieving a homogeneous and small demagnetising field, an elliptical shape of the AMR array is proposed [8]. By applying a flipping field H_F , the direction of M_s in the AMR element can be inverted — this is very useful to overcome offset problems. The schematic evaluation arrangement is shown in Fig. 4. Using a compensation coil at the output of the integrator, the sensor can be operated in zero magnetic field. The linear output response (voltage V_0 versus applied field H_a) is proportional (resistor R) to the compensation coil current. Both flipping and compensation coils are thin film conductors in a meanderic form; they are also shown schematically in Fig. 4.

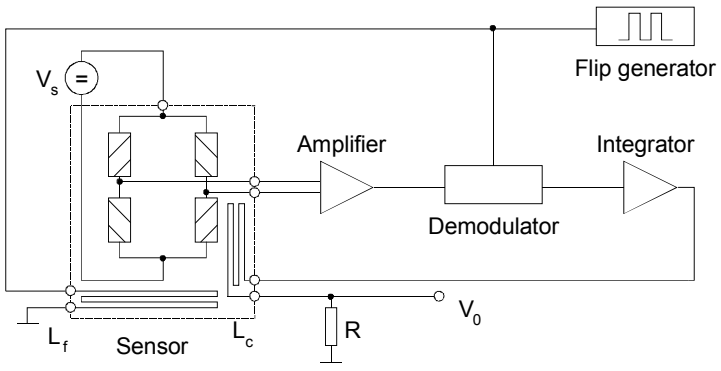

Fig. 4: Electronic evaluation circuit with flip- (L_f) and compensation (L_c) coils

[2] According to [3] there are two definitions of the sensitivity of an AMR sensor in a bridge arrangement: 1. $S_0 = \mathrm{d}U_A/\mathrm{d}H_y/U_B$, and 2. $S_U = U_{max} \times \mathrm{d}U_A/\mathrm{d}H_y/U_B$. The advantage of the second definition is that it also takes into account the maximum energy dissipation ($P_{max} = U_{B,max}^2/R$) in the sensor. The supply voltage can not be made arbitrarily high. For comparison of the sensitivities of various sensors, we use the first definition in this paper, as is done through most of the literature.

Sensor layout and film technology

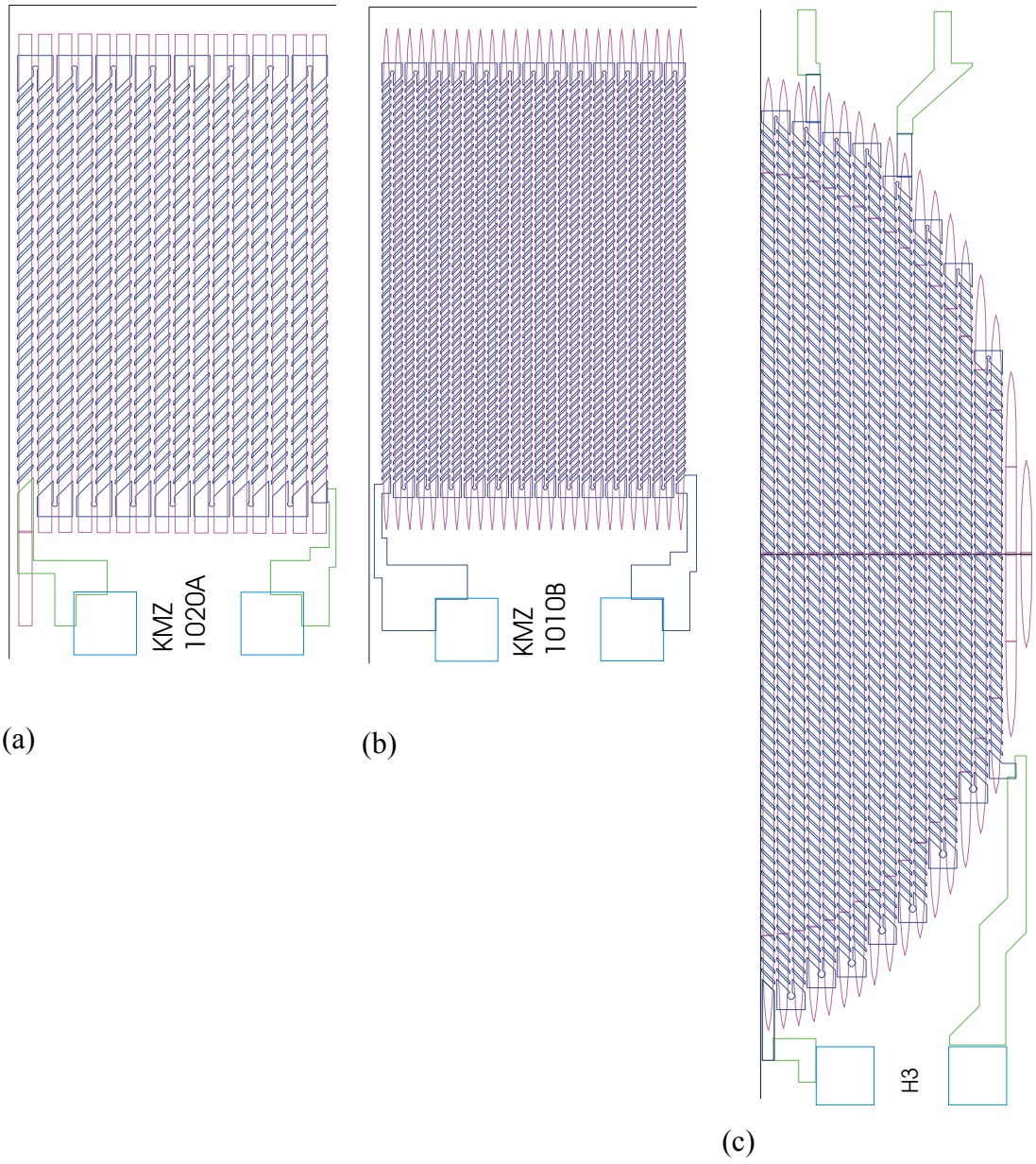

Fig. 5: Layout of KMZ 1020A (a) one of four bridge resistors, active area of the permalloy strips: 470 × 770 µm^2, KMZ 1010B (b), and H3 (c) half bridge; long axis length: 1760 µm; the AMR films are covered with barber poles (/); two bonding pads (□) belong to one resistor.

Three layouts with rectangular permalloy strips of different width and separation distance have been investigated (see Fig. 5):

a) KMZ1020A: Width 20 µm (tapering off at both ends), distance 10 µm, R_0 = 1.70 kΩ, S_0 = 3.31 (mV/V)/(kA/m), H_F = 400 A/m.

b) KMZ1010B: Width 10 µm, distance 10 µm, R_0 = 5.63 kΩ, S_0 = 1.36 (mV/V)/(kA/m), H_F = 2000 A/m.

c) H3: Width 10 µm (tapering off at the ends), distance 10 µm, R_0 = 5.63 kΩ, S_0 = 1.36 (mV/V)/(kA/m), H_F = 2000 A/m, overall elliptical shape. Ellipse axes are a = 1760 µm and b = 1000 µm.

The total sensor area was 1 × 2 mm^2 for each layout. The AMR film was characterised by $\Delta\rho/\rho$ = 1.52% and H_0 = 600 A/m.

The magnetoresistive films have been deposited by DC cathode sputtering using a triode set-up. This triode sputtering system has some advantages compared to a simple diode set-up, because the plasma is sustained independently of the target voltage, and it can be easily concentrated in the centre of the chamber by a magnetic field generated through an external coil. The arrangement is schematically shown in Fig. 6. A target consisting of 81% Ni and 19% Fe (magnetostriction free) has been used. It is connected to a negative potential of V_T = – 800 V. A negative substrate bias voltage of V_B = – 60 V and an anode voltage of V_A = +50 V are applied. The currents indicated in Fig. 6 are I_A = 3.5 A, I_C = 45 A and I_{COIL} = 2 – 6 A. The glass chamber is evacuated by a turbomolecular pump to a residual gas pressure of about 10^{-7} mbar and the argon pressure is adjusted to 2×10^{-3} mbar. During film deposition the substrates are heated and exposed to a constant magnetic field. It is important that the direction of the magnetic field is parallel to the substrate plane. The substrates are taken out of the vacuum chamber as soon as they are completely cooled down to room temperature.

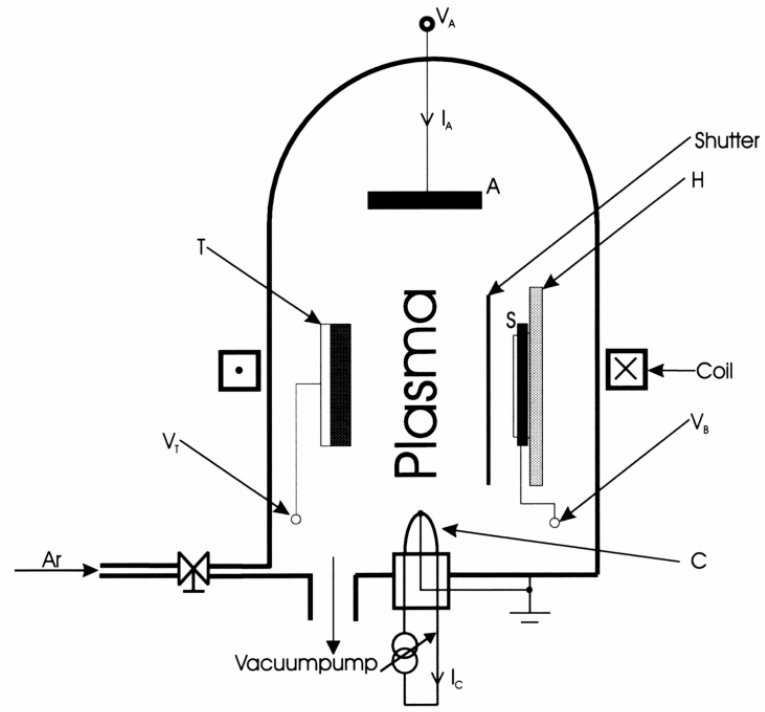

Fig. 6: DC sputtering set-up (triode system), A: anode, T: target, C: hot filament cathode, S: substrate, H: heater.

The following main parameters can influence the properties of sputtered magnetoresistive films and have therefore been varied: Method of substrate passivation, temperatures of target (T_T) and substrate (T_S), distance $a_{T–S}$ between target and substrate, and the film thickness d. Furthermore, the resistivity of the film depends also on the strength of the applied magnetic field, the direction of the field, and the film deposition rate. Film thickness measurements have been carried out with an Inficon quartz crystal film thickness monitor. The resistance has been measured by a four-wire method.

The substrate material is silicon (3" and 4" wafer with (100) orientation). The wafer surface has been passivated by a 0.5 – 0.8 µm insulation layer, consisting either of a thermal silicon dioxide or a low stress silicon nitride deposited by a PECVD process at low temperature. Sputtered silicon dioxide has also been used in some experiments.

Measurements and results

The results indicate an increasing AMR effect Δρ/ρ with decreasing ρ. Both T_S and T_T have a positive influence on the AMR effect. The target–substrate distance has been varied between 36 mm and 60 mm, yielding a change in the AMR effect by ± 0.2%. The optimum $a_{T–S}$ is in the range between 38mm and 42mm. The optimum film thickness d was about 50 nm. With these parameters we achieved an AMR effect of Δρ/ρ = 3.93% [9]. Reducing d to 20 nm, which has often been reported to be the optimum for permalloy, e.g. [10], yields a decrease of the AMR effect by 0.5%. The magnetic behaviour depends strongly on the thickness d. This is demonstrated by magnetisation curves measured by the magneto-optical Kerr effect. Reducing d from 50 nm to 20 nm, both the easy axis coercivity and the hard axis coercivity increase [6].

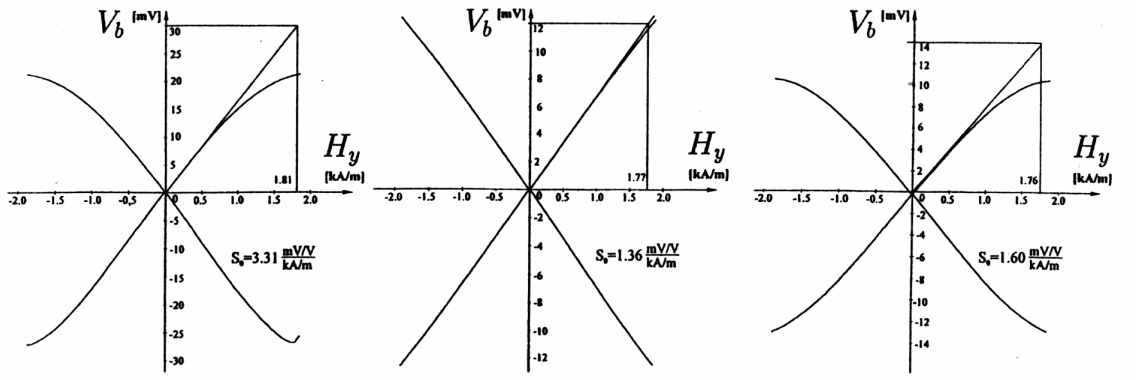

(a) (b) (c)

Fig. 7: Sensitivity of KMZ 1020A (a), KMZ 1010B (b), and H3 (c); the output voltage Vb of the half bridge versus the applied field H_y could be about 8 times greater using a full bridge with an elliptical resistor layout rotated by 90° compared to Fig. 5 (c).

Depending both on the demagnetising factor of the single strips and the total area, the sensitivity of KMZ1020A is about 2.5 times of that of the KMZ1010B. The layout H3 was designed as a half bridge and therefore its sensitivity is half of KMZ1020A. The

sensor characteristic of both magnetic states are shown in Fig. 7. Rotating the elliptical shape by 90° (in order to align the applied field perpendicular to the permalloy strips but parallel to the long axis of the ellipse) results in a sensitivity increase by $(N_b/N_a)^2$, where N_a is the demagnetising factor in the long axis direction and N_b is the demagnetising factor in the short axis direction of the ellipse. Furthermore, the signal/noise ratio is improved by achieving more homogeneous fields as compared to the KMZ layouts, which is shown in Fig. 8.

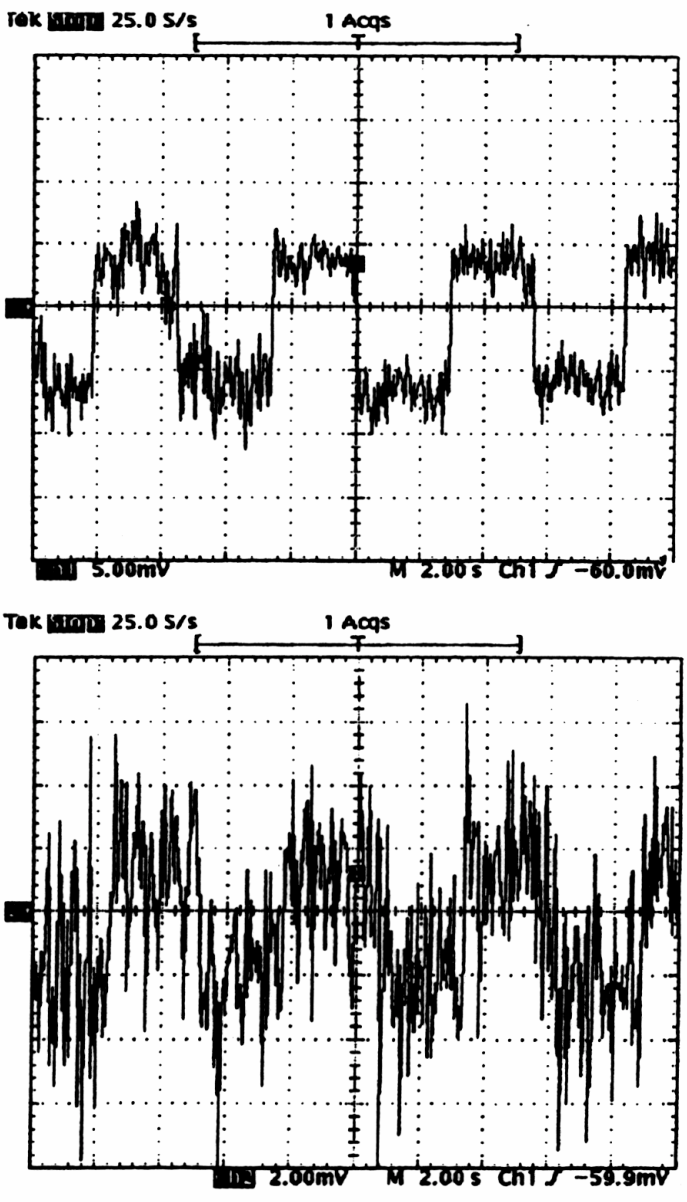

Fig. 8: Output voltage V_b versus time (2 s/div.) of the sensors H3 (5 mV/div., above) and KMZ 1010B (2 mV/div., below).

Conclusions

For a high sensitivity, the hard axis coercivity should be near zero. This is demonstrated by our recent results which show almost ideal Stoner-Wohlfahrth rotation of the spontaneous magnetisation ($H_{c;\,e:a}$ = 162 A/m, $H_{c;\,h:a} \approx 0$). Providing a high $\Delta\rho/\rho$ = 3.43%, this sample is considered to be an optimum AMR sensor material [9] (the samples of maximum $\Delta\rho/\rho$ up to 3.93% have a larger hard axis coercivity of about 20 A/m).

Using furthermore a Wheatstone bridge arrangement of elliptical shape with barber pole-structured magnetoresistors (see Fig. 5, layout H3, rotated by 90°, which means that the permalloy strips are orientated along the short axis of the ellipse) gives a sensitivity of 0.5 µV/nT at a supply voltage of 10V. The bandwidth depends on the flip frequency; in the case of a long flipping period, the bandwidth could be in the MHz range.

With these sensors it is possible to detect the distortion of the earth's magnetic field — caused by ferromagnetic objects which have to be located — with a gradiometer arrangement. Various industrial and automotive electronics applications can be considered because of the low production cost.

Acknowledgements

The authors are grateful to Prof. W. Fallmann and to Prof. G. Fasching for making these investigations possible, and to P. Aigner, R. Kloibhofer, and W. Krenn for technical assistance. Financial support was provided by the company Dipl.-Ing. Hans Schiebel Elektronische Geräte GmbH and by the Forschungsförderungsfonds für die Gewerbliche Wirtschaft (FFF) under grant no. 3/9893.

References

[1] Thomson, W.: Proc. R. Soc. London A 8 (1857), 546 – 550.

[2] Baibich, M. N. et al.: Phys. Rev. Lett. 61 (1988), 2472.

[3] Dibbern, U.: Magnetoresistive Sensors; in: G. opel, W., Hesse, J. und Zemel J. N. (ed.): Sensors, Vol. 5, Magnetic Sensors (Vol. Editors.: Boll, R. und Overshott, K. J.), 342 – 379. Weinheim: VCH 1989.

[4] Fasching, G. M.: Werkstoffe für die Elektrotechnik. 3. Auflage. Wien – New York: Springer 1994.

[5] Hauser, H. and Fulmek, P.: The Effect of Mechanical Stress on the Magnetization Curves of Ni- and FeSi-Single Crystals at Strong Fields. IEEE Trans. Magn. 28 (1992), 1815 – 1825.

[6] Fulmek, P. and Hauser, H.: Simulation of the Magnetization Process in Anisotropic Ferromagnetic Materials by Energy Areas. Elsevier Studies in Applied Electromagnetics in Materials, Vol. 5 (1993), 327 – 330.

[7] Feng, J. S. Y., Romankiw, L. T. and Thompson, D. A.: Magnetic self-bias in the barber pole MR structure. IEEE Trans. Magn. 13 (1977) S. 1466 bis 1468.

[8] Hauser, H.: Magnetfeldsensor II. Austrian Pat. Appl. No. 1928/96 (1996).

[9] Aigner, P., Stangl, G. and Hauser, H.: Cathode Sputtered Permalloy Films of High Anisotropic Magnetoresistive Effect. J. Phys. IV 8 (1998) 461 – 464.

[10] Song, Y. J. and Joo, S. K.: Magnetoresistance and magnetic anisotropy of permalloy based multilayers. IEEE Trans. Magn. 32 (1996), 5 – 8.